IEEE Open Access Journal of
Power and Energy

Received 31 March 2026; revised 22 June 2026; accepted 27 July 2026. Date of publication 5 August 2026; date of current version 14 August 2026.

*Digital Object Identifier 10.1109/OAJPE.2026.3720546*

# A Novel Dynamic Phasor-Based Mathematical Framework for Hybrid AC/DC Power System Simulation

**SAIF ALSARAYREH[1] (Student Member, IEEE), ROBERT DIMITROVSKI[2], AND ALEKSANDRA LEKIĆ[1] (Senior Member, IEEE)**

[1]Faculty of Electrical Engineering, Mathematics, and Computer Science, TU Delft, CD, 2618 Delft, The Netherlands
[2]TenneT TSO GmbH, 95448 Bayreuth, Germany

CORRESPONDING AUTHOR: S. ALSARAYREH (S.T.S.Alsarayreh@tudelft.nl)

This work was supported by the Collaborative Research for Energy SYstem Modelling (CRESYM) Project Harmony (https://cresym.eu/harmony/).

**ABSTRACT** Modern power systems with high penetration of inverter-based resources (IBRs) exhibit fast dynamics and complex harmonic interactions that challenge conventional modelling tools. Electromagnetic transient (EMT) simulations provide high fidelity but are computationally demanding for large-scale studies due to small time-step requirements, whereas conventional phasor-domain models neglect harmonic and higher-frequency effects to allow for larger time-steps. This paper proposes a unified dynamic-phasor-based framework (*DQsym*), implemented as a MATLAB/Simulink library, that combines dynamic phasors with multiple rotating reference frames and defines explicit algebraic rules for harmonic-domain operations compatible with state-space formulations, enabling systematic assembly of interconnected system-level models beyond isolated component representations. The formulation supports modelling across multiple harmonic orders and is expressed in state space, providing a natural pathway for future integration with small-signal analysis and control design tools, although such extensions are outside the scope of this paper. The approach is validated through: 1) benchmark case demonstrating higher-order harmonic modelling capability and 2) simulations of an IEEE 9-bus system expanded with point-to-point HVDC transmission based on a modular multilevel converter (MMC), where the framework reproduces fundamental and second-harmonic dynamics indicating that *DQsym* reproduces the overall harmonic pattern and closely matches the fundamental component compared with EMT results. The proposed framework provides a structured and accurate harmonic-domain modelling tool for the analysis of IBR-rich power systems.

**INDEX TERMS** Dynamic phasor, harmonics, HVDC, modular-multilevel (MMC).

## I. INTRODUCTION

THE integration of inverter-based resources (IBRs), such as wind turbines, solar photovoltaic systems, and battery storage, is central to the transition to sustainable power systems. Unlike conventional synchronous generators, IBRs rely on fast-switching power electronic converters and control systems that introduce dynamics across a wide range of time scales, from microsecond–millisecond electromagnetic effects to slower electromechanical dynamics [1]. Converter switching and control actions also generate harmonic and interharmonic components, increasing the complexity of hybrid AC/DC power system (HPS) studies [2]. Accurate modelling of these multi-timescale and harmonic effects is therefore essential for modern power system analysis.

A key requirement is the ability to represent harmonic content introduced by IBRs and its propagation through the network [2]. Transmission system operators traditionally rely on Root-Mean-Square (RMS) phasor-domain simulations that focus on fundamental-frequency quantities. However, IBR-dominated systems exhibit sub- and super-synchronous dynamics that require electromagnetic transient (EMT) and harmonic simulations for detailed assessment [3], [4]. EMT tools provide high accuracy by modelling switching behavior and nonlinear effects in the *abc* frame, but they require very small time steps and significant computational effort. Dynamic phasor (DP) modelling has therefore emerged as an intermediate approach, representing signals using time-varying Fourier coefficients to capture selected harmonic components while allowing larger simulation time steps [5], [6], [7], [8], [9], [10], [11].

Although DP-based models have been developed for individual components, such as synchronous generators, multi-converter systems, and grid-forming converters [12], [13], [14], [15], less attention has been given to systematic system-level modelling. Existing approaches are often code-based for real-time simulation [16], modular implementations [17], or rely on equivalent switching functions [18]. In many cases, the required dynamic phasor operations—multiplication, integration, and summation—are not expressed in a state-space form, making it difficult to assemble interconnected AC/DC networks in a structured and repeatable manner.

To address this gap, this paper proposes a unified simulation framework termed *DQsym*, which combines dynamic phasors with multiple rotating *dq* reference frames to represent positive-, negative-, and zero-sequence harmonic components in a consistent state-space structure. The framework enables systematic assembly of interconnected AC/DC systems while preserving selected harmonic dynamics. An open-source MATLAB/Simulink implementation of the *DQsym* library is described separately in [19]. The present paper establishes the mathematical foundations underlying the framework, specifically the harmonic convolution theorem, the integration rule, and provides validation against EMT simulations across multiple test cases of increasing complexity.

The proposed approach is validated through two case studies: a benchmark harmonic interaction example and an IEEE 9-bus system extended with point-to-point MMC-based HVDC transmission. The results show close agreement with EMT simulations for both fundamental and second-harmonic dynamics.

This paper makes the following contributions:

- A unified simulation framework, *DQsym*, combining dynamic phasors with multiple rotating *dq* reference frames for fundamental and selected harmonic modelling, structurally supporting both balanced and unbalanced conditions through positive-, negative-, and zero-sequence decomposition.
- State-space formulation of dynamic phasor operations, enabling structured and repeatable modelling of interconnected AC/DC systems.
- Modular system assembly approach for consistent harmonic modelling across subsystems.
- Validation using benchmark studies and an IEEE 9-bus MMC-HVDC system with close agreement to EMT results.

The framework preserves a state-space structure, providing a foundation for future stability and control analysis.

## II. DYNAMIC PHASOR THEORY

DPs provide a compact, frequency-shifted representation of signals that captures both amplitude and phase variations over time. Unlike static phasors — which assume a purely sinusoidal, steady-state waveform — DPs generalise this concept to non-stationary, harmonically rich signals by treating the Fourier coefficients themselves as time-varying quantities. The goal is a structured ODE representation that retains harmonic content with far fewer state variables than a full EMT model.

For a nearly periodic waveform $x(\tau)$ observed over the sliding window $(t-T, t)$, the $k^{\text{th}}$ DP is defined as the time-localised Fourier projection

$$X_k(t) \triangleq \langle x \rangle_k(t) = \frac{1}{T}\int_{t-T}^{t} x(\tau)\, e^{-jk\omega_c\tau}\, d\tau, \tag{1}$$

where $\omega_c = 2\pi/T$ is the fundamental angular frequency. Given the coefficients $\langle x\rangle_k$, the original signal is recovered via the generalised Fourier series

$$x(\tau) = \sum_{k=-\infty}^{\infty} \langle x\rangle_k(t)\, e^{jk\omega_c\tau}. \tag{2}$$

Eq. (1) computes DPs from a signal, and Eq. (2) reconstructs the signal from its DPs. Under steady-state conditions, the coefficients $\langle x\rangle_k(t)$ converge to constant (DC-like) values, yielding a time-invariant representation that directly facilitates eigenvalue-based analysis.

Three properties, inherited from the Fourier series, are central to constructing DP-based state-space models [9]:

- **Time derivative:**
$$\frac{d\langle x\rangle_k}{dt} = \left\langle \frac{dx}{dt}\right\rangle_k - jk\omega_c\langle x\rangle_k. \tag{3}$$
- **Multiplication (harmonic convolution):**
$$\langle xy\rangle_k(t) = \sum_{i=-\infty}^{\infty} \langle x\rangle_{k-i}(t)\,\langle y\rangle_i(t). \tag{4}$$
- **Conjugate symmetry:** For any real-valued signal $x(\tau)$,
$$\langle x\rangle_{-k}(t) = \langle x\rangle_k^*(t). \tag{5}$$

The symmetry rule implies that negative-index coefficients carry no additional information, allowing the two-sided series in Eq. (2), truncated to $|k| \le N$, to be replaced by a one-sided real-valued form. Pairing the $\pm n$ terms and applying Euler's identity yields

$$x(\tau) = \langle x\rangle_0(t) + \sum_{n=1}^{N} 2|\langle x\rangle_n(t)|\cos\bigl(n\omega_c\tau + \arg\langle x\rangle_n(t)\bigr), \tag{6}$$

reducing the number of independent complex coefficients from $2N+1$ to $N+1$. Throughout this work, DQsym adopts this one-sided convention, with $n = 0$ denoting the DC component and $n = 1,\ldots,N$ indexing the retained harmonics.

For implementation in a simulation framework, it is convenient to work with real-valued state variables. Any DP

$\langle x\rangle_n(t)$ can be decomposed into in-phase ($x_{In}$) and quadrature ($x_{Qn}$) components, so that the signal representation of Eq. (6), evaluated at $\tau = t$, becomes

$$x(t) = a_0 + \sum_{n=1}^{N} x_{In}(t)\cos(n\omega_c t) - x_{Qn}(t)\sin(n\omega_c t), \quad (7)$$

with $a_0 = \langle x\rangle_0(t)$. The corresponding complex DP is then

$$\langle x\rangle_n(t) = x_{In}(t) + j\,x_{Qn}(t) = A_n(t)\,e^{j\theta_n(t)}, \quad (8)$$

where $A_n(t) = 2|\langle x\rangle_n(t)|$ is the instantaneous amplitude and $\theta_n(t) = \arg\langle x\rangle_n(t)$ is the instantaneous phase, consistent with the one-sided identification in Eq. (6). A single harmonic component is recovered from its DP by remodulation and taking the real part:

$$x_n(t) = \Re\left\{\langle x\rangle_n(t)\,e^{jn\omega_c t}\right\} = A_n(t)\cos\bigl(n\omega_c t + \theta_n(t)\bigr), \quad (9)$$

with the full signal recovered by summing over all retained harmonics as in Eq. (7).

## III. PROPOSED FRAMEWORK

This section presents the *DQsym* framework, beginning with the mathematical foundation of DPs, followed by the state-space formulation and its integration into *DQsym* framework.

### A. TRANSFORMATION OF DYNAMIC PHASOR QUANTITIES FROM ABC TO DQSYM FRAME

As stated DPs ($X_k(t)$) are time-varying Fourier coefficients, slowly varying when the signal is near-periodic around a base frequency. Their in-phase ($x_I(t) = \Re\{X_k(t)\}$) and quadrature ($x_Q(t) = \Im\{X_k(t)\}$) components are orthogonal, which allows each phasor to represent a specific $k^{\text{th}}$ harmonic without coupling formation with other harmonic DPs. These properties form the basis for transforming DP quantities from the *abc* frame to the rotating *dq*0 frame.

Considering a general three-phase signal $\vec{x}_{abc}(t) = \left[x_a(t)\ x_b(t)\ x_c(t)\right]^T$, that may be unbalanced, applying the classical symmetrical component transformation $T_{pnz}$, the three-phase signals are decomposed into positive-, negative-, and zero-sequence components:

$$\vec{x}_{pnz}(t) = T_{pnz}\cdot\vec{x}_{abc}(t) = \vec{x}_p(t) + \vec{x}_n(t) + \vec{x}_z(t), \quad (10)$$

where

$$T_{pnz} = \frac{1}{3}\begin{bmatrix} 1 & a & a^2 \\ 1 & a^2 & a \\ 1 & 1 & 1 \end{bmatrix}, \quad a = e^{j\frac{2\pi}{3}}. \quad (11)$$

This decomposition is what allows DQsym to structurally represent unbalanced three-phase conditions, since the negative- and zero-sequence components become nonzero precisely when the signal departs from balanced symmetry, consistent with sequence-domain dynamic phasor approaches validated for power-electronic systems under unbalanced conditions [20]. All validation cases presented in this paper (Section IV) involve balanced operation; demonstrating this capability under unbalanced conditions is identified as future work.

In order to describe it in a simpler manner, let us assume that signal $\vec{x}_{abc}(t)$ is a sinusoid with amplitude $X_i(t)$ and phase $\theta_i(t)$, $i \in \{a, b, c\}$, displaced by 120°:

$$\begin{bmatrix} x_a \\ x_b \\ x_c \end{bmatrix} = \begin{bmatrix} X_a(t)\cos(\omega t + \theta_a \\ X_b(t)\cos\left(\omega t + \theta_b - \frac{2\pi}{3}\right) \\ X_c(t)\cos\left(\omega t + \theta_c + \frac{2\pi}{3}\right) \end{bmatrix}. \quad (12)$$

Then, based on equation (10), each component can be expressed as

$$\vec{x}_j(t) = X_j\cdot\begin{bmatrix} \cos(\omega t + \theta_j) \\ \cos\left(\omega t + \theta_j + i\frac{2\pi}{3}\right) \\ \cos\left(\omega t + \theta_j - i\frac{2\pi}{3}\right) \end{bmatrix}, i = \begin{cases} -1, & j = p \\ 1, & j = n \\ 0, & j = z \end{cases}. \quad (13)$$

or equivalently in phasor form [11]:

$$\vec{x}_j(t) = X_j\cdot\begin{bmatrix} e^{j(\omega t + \theta_j)} \\ e^{j\left(\omega t + \theta_j + \frac{2i\pi}{3}\right)} \\ e^{j\left(\omega t + \theta_j - \frac{2i\pi}{3}\right)} \end{bmatrix}. \quad (14)$$

Mapping the three-phase system into the stationary $\alpha\beta0$ frame using Clarke transformation as:

$$\vec{x}_{\alpha\beta0,j}(t) = T_c\cdot\vec{x}_j(t), \quad T_c = \frac{2}{3}\begin{bmatrix} 1 & -\frac{1}{2} & -\frac{1}{2} \\ 0 & \frac{\sqrt{3}}{2} & -\frac{\sqrt{3}}{2} \\ \frac{1}{2} & \frac{1}{2} & \frac{1}{2} \end{bmatrix}, \quad (15)$$

which is in complex form:

$$\begin{bmatrix} x_{\alpha\beta,p} \\ x_{\alpha\beta,n} \\ x_{0,z} \end{bmatrix} = \begin{bmatrix} X_p e^{j(\omega t + \theta_p)} \\ X_n e^{-j(\omega t + \theta_n)} \\ X_z e^{j(\omega t + \theta_z)} \end{bmatrix}. \quad (16)$$

Extracting the DPs requires a frequency shift [11]:

$$\begin{bmatrix} \langle x_{\alpha\beta,p}\rangle \\ \langle x_{\alpha\beta,n}\rangle \\ \langle x_{0,z}\rangle \end{bmatrix} = \begin{bmatrix} X_p e^{j\theta_p} \\ X_n e^{-j\theta_n} \\ X_z e^{j\theta_z} \end{bmatrix}. \quad (17)$$

The negative-sequence phasor may equivalently be expressed in a positively rotating frame:

$$\langle x_{\alpha\beta,n}\rangle = \langle x_{\alpha\beta,n}\rangle^* = X_n e^{j\theta_n}.$$

Finally, the Park transformation rotates the $\alpha\beta0$ components into the $dq0$ frame:

$$\begin{bmatrix} \langle x_{dq,p}\rangle_k \\ \langle x_{dq,n}\rangle_k \\ \langle x_{dq,z}\rangle_k \end{bmatrix} = \underbrace{\begin{bmatrix} e^{-j\theta} & 0 & 0 \\ 0 & e^{-j\theta} & 0 \\ 0 & 0 & 1 \end{bmatrix}}_{T_{Rot}} \begin{bmatrix} \langle x_{\alpha\beta,p}\rangle_k \\ \langle x_{\alpha\beta,n}\rangle_k^* \\ \langle x_{0,z}\rangle_k \end{bmatrix}. \quad (18)$$

Thus, in *DQsym* form is:

$$\begin{bmatrix} \langle x_{dq,p}\rangle_k \\ \langle x_{dq,n}\rangle_k \\ \langle x_{dq,z}\rangle_k \end{bmatrix} = \begin{bmatrix} X_k^p e^{j\theta_k^p} \\ X_k^n e^{j\theta_k^n} \\ X_k^z e^{j\theta_k^z} \end{bmatrix} = \begin{bmatrix} \mathbf{x}_d^p(k) + j\mathbf{x}_q^p(k) \\ \mathbf{x}_d^n(k) + j\mathbf{x}_q^n(k) \\ \mathbf{x}_d^z(k) + j\mathbf{x}_q^z(k) \end{bmatrix}. \quad (19)$$

[11], [20] shows that this procedure maps DPs in the *abc* frame into the *DQsym* frame by (i) applying the symmetrical component transformation $T_{pnz}$, and (ii) rotating the positive- and negative-sequence phasors by $-\theta$ via $T_{Rot}$. Equation (20) summarizes this transformation: DPs are first constructed in the *abc* frame using in-phase and quadrature coefficients ($C^c$ and $C^s$), then transformed into symmetrical components via $T_{pnz}$, and finally rotated into the *DQsym* frame via $T_{Rot}$.

$$\begin{bmatrix} \mathbf{C}_k^c + j\mathbf{C}_k^s \\ \mathbf{C}_k^c + j\mathbf{C}_k^s \\ \mathbf{C}_k^c + j\mathbf{C}_k^s \end{bmatrix} = \begin{bmatrix} \langle x_a \rangle_k \\ \langle x_b \rangle_k \\ \langle x_c \rangle_k \end{bmatrix} \xRightarrow{T_{pnz}} \begin{bmatrix} \langle x_{\alpha\beta,p} \rangle_k \\ \langle x_{\alpha\beta,n} \rangle_k^* \\ \langle x_{0,z} \rangle_k \end{bmatrix},$$
$$T_{Rot} \begin{bmatrix} \langle x_{\alpha\beta,p} \rangle_k \\ \langle x_{\alpha\beta,n} \rangle_k^* \\ \langle x_{0,z} \rangle_k \end{bmatrix} \Rightarrow \begin{bmatrix} \langle x_{dq,p} \rangle_k \\ \langle x_{dq,n} \rangle_k \\ \langle x_{dq,z} \rangle_k \end{bmatrix} \tag{20}$$

### B. MATHEMATICAL OPERATIONS

The following set of mathematical operations—summation, multiplication, and integration—form the basis of the DQsym approach and enable its application to full system simulations.

#### 1) SUMMATION

Summing DPs in *DQsym* frame adheres to complex-number rules with no change in the form of the inputs or additional operations needed (i.e. simple elementwise additivity), as follows:

$$\begin{bmatrix} \mathbf{x}^p(0) & \cdots & \mathbf{x}^p(n) \\ \mathbf{x}^n(0) & \cdots & \mathbf{x}^n(n) \\ \mathbf{x}^z(0) & \cdots & \mathbf{x}^z(n) \end{bmatrix} + \begin{bmatrix} \mathbf{y}^p(0) & \cdots & \mathbf{y}^p(n) \\ \mathbf{y}^n(0) & \cdots & \mathbf{y}^n(n) \\ \mathbf{y}^z(0) & \cdots & \mathbf{y}^z(n) \end{bmatrix}$$
$$= \begin{bmatrix} \mathbf{z}^p(0) & \cdots & \mathbf{z}^p(n) \\ \mathbf{z}^n(0) & \cdots & \mathbf{z}^n(n) \\ \mathbf{z}^z(0) & \cdots & \mathbf{z}^z(n) \end{bmatrix} \tag{21}$$

where $z_{d,q}^{p,n,z}(i) = x_{d,q}^{p,n,z}(i) + y_{d,q}^{p,n,z}(i)$, for $i \in \{0, \ldots, n\}$.

#### 2) MULTIPLICATION

Any time-varying signal can be represented as an infinite sum of sine and cosine functions at integer multiples of the fundamental frequency $\omega_c$, and each sinusoid $\sin(n\omega_c t)$ or $\cos(n\omega_c t)$ corresponds to the $n^{\text{th}}$ harmonic of $x(t)$. This expansion is known as the trigonometric Fourier series of $x(t)$, with coefficients $a_n$ and $b_n$ denoting the Fourier sine and cosine coefficients. The coefficient $a_0$ represents the DC component (average value) of the signal, while $a_n$ and $b_n$ ($n \neq 0$) define the amplitudes of the sinusoidal terms that constitute the AC component:

$$x(t) = a_0 + a_1 \cos \omega_0 t + b_1 \sin \omega_0 t + a_2 \cos 2\omega_0 t + b_2 \sin 2\omega_0 t + a_3 \cos 3\omega_0 t + b_3 \sin 3\omega_0 t + \cdots \tag{22}$$

or

$$x(t) = \underbrace{a_0}_{\text{dc}} + \underbrace{\sum_{n=1}^{\infty} (a_n \cos n\omega_0 t + b_n \sin n\omega_0 t)}_{\text{ac}}. \tag{23}$$

*Theorem 1:* The product of two periodic signals with fundamental frequency $\omega$ represented by a truncated Fourier series of order $N$:

$$x(t) = a_0 + \sum_{i=1}^{N} \left( a_i^s \sin(i\omega t) + a_i^c \cos(i\omega t) \right), \tag{24}$$
$$y(t) = b_0 + \sum_{j=1}^{N} \left( b_j^s \sin(j\omega t) + b_j^c \cos(j\omega t) \right). \tag{25}$$

denoted as $z(t) = x(t)y(t)$ can be expressed as

$$z(t) = C_0 + \sum_{k=1}^{2N} \left( C_k^s \sin(k\omega t) + C_k^c \cos(k\omega t) \right), \tag{26}$$

where the coefficients $C_0$, $C_k^s$, and $C_k^c$, for $k \in \{1, \ldots 2N\}$, are given in (27), as shown at the bottom of the next page.

The proof of this theorem and derivation for (27) are provided in the appendix. The derivation highlights the similarity between the Fourier coefficients of the product and the in-phase and quadrature components in dynamic phasor theory. Hence, dynamic phasors can be constructed directly from $C_k^c$ and $C_k^s$ for each harmonic $k$, with $C_0$ representing the DC term. The overall multiplication process is illustrated in Fig. 1, and it includes the following steps:

- Transform the input signals $x_{dq}^{p,n,z}$ and $y_{dq}^{p,n,z}$ into their phase-domain representations $x_{dq}^{a,b,c}$ and $y_{dq}^{a,b,c}$.
- Extract the sine and cosine Fourier coefficients for each phase of the input signals.
- Perform phase-by-phase multiplication, computing the coefficient products $C_0$, $C_k^s$, and $C_k^c$ using (27).
- Collect the resulting terms and transform the output $z_{dq}^{a,b,c}$ back to the $z_{dq}^{p,n,z}$ representation.

#### 3) INTEGRATION

Time-varying signals up to the $n^{\text{th}}$ harmonic order can be expressed using a Fourier series

$$f(t) = a_0 + \sum_{n=1}^{\infty} (a_n \cos(n\omega_0 t) + b_n \sin(n\omega_0 t)) \tag{28}$$

Any antiderivative $F(t)$ can be obtained term-by-term based on the integration theorem of the Fourier series:

$$F(t) = a_0\, t + \sum_{n=1}^{\infty} \frac{a_n}{n\omega_0} \sin(n\omega_0 t) - \sum_{n=1}^{\infty} \frac{b_n}{n\omega_0} \cos(n\omega_0 t), \tag{29}$$

which corresponds to the standard integration of the Fourier coefficients. Considering $f_{dq}$ in complex form, i.e., $f_d(n) + jf_q(n)$, integration with respect to time yields (30). In contrast, when $f_{dq}$ is expressed in DP representation, the factor $e^{jn\omega_0 t}$ is removed, and integration yields (31), which demonstrates that integrating DPs in $dq$ form introduces cross-coupling between the $d$ and $q$ components.

$$\int f_{dq}(n) e^{jn\omega_0 t} dt$$
$$= \left( f_d(n) + jf_q(n) \right) \int e^{jn\omega_0 t} dt$$

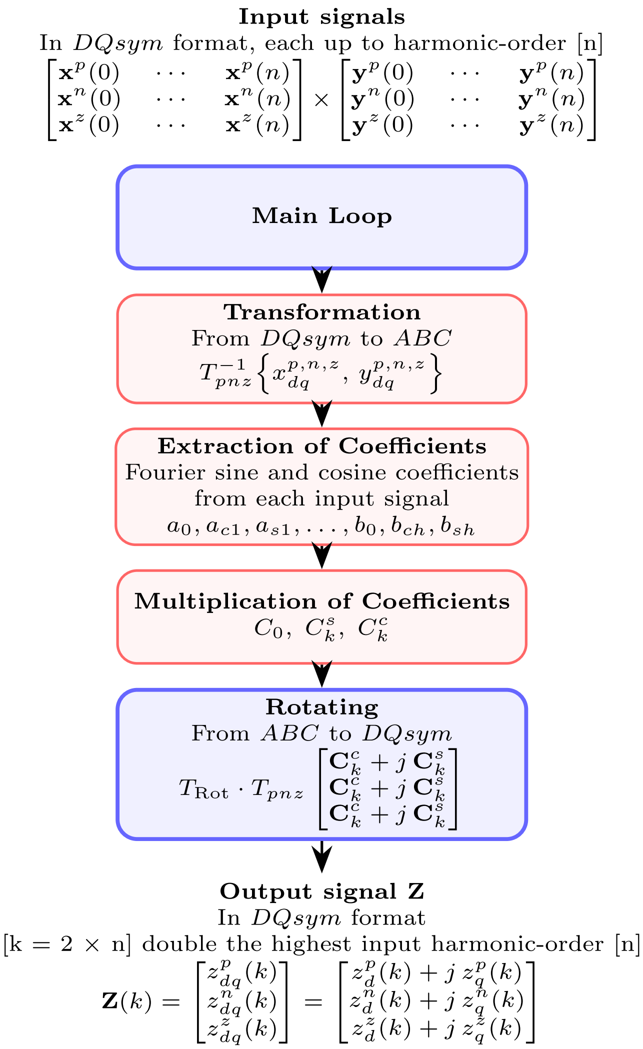


**FIGURE 1. Flowchart of the multiplication algorithm for harmonic-rich signals $x_{dqn}^{p,n,z}(i)$ and $y_{dqn}^{p,n,z}(i)$.**

$$= \left(f_d(n) + jf_q(n)\right)\frac{-j}{n\omega_0}e^{jn\omega_0 t} + C \tag{30}$$

$$\langle f_{dq}\rangle \Rightarrow \boxed{\int} \Rightarrow \langle F_{dq}\rangle = \left(f_d(n) + jf_q(n)\right)\frac{-j}{n\omega_0} + C \tag{31}$$

This process can be generalized to the integration of $\langle f_{dq}^{p,n,z}\rangle$, yielding $\langle F_{dq}^{p,n,z}\rangle$. Both vectors are equal in dimension up to the $n^{\text{th}}$ harmonic order.

### C. STATE-SPACE FORMULATION FOR DQSYM

In EMT simulations, system dynamics are described by differential equations written in state-space form,

$$\dot{x}(t) = Ax(t) + Bu(t), \qquad y(t) = Cx(t) + Du(t), \tag{32}$$

Applying the dynamic phasor derivative property, the system at harmonic order $k$ becomes

$$\begin{aligned} \dot{X}_k(t) &= \left(A_{dqn} - jk\omega_s I\right)X_k(t) + B_{dqn}U_k(t), \\ Y_k(t) &= C_{dqn}X_k(t) + D_{dqn}U_k(t), \end{aligned} \tag{33}$$

where $X_k(t)$ and $U_k(t)$ are the dynamic phasor states and inputs, and $Y_k(t)$ is the output. In the present approach, a state-space model is first derived for each individual component of the network using its governing differential equations. The overall system model is then obtained by augmenting these individual state-space representations into a single, unified set of equations. The complete system is expressed in standard state-space form, resulting in the global $A$, $B$, $C$, and $D$ matrices. The state-space block also provides the ability to include switching activity, as the block houses an algorithm to update the system matrices to reflect the effect of the switching event on the output quantities, as seen in Fig. 2. This approach enables consistent and extensible modelling of dynamic components across different system configurations.

## IV. VALIDATION

### A. MULTIPLICATION OF HARMONIC-RICH SIGNALS

An example of the multiplication of two randomly generated harmonic-rich signals up to the 5$^{\text{th}}$ order, as defined in (34), is shown in Fig. 3 using blocks from the *DQsym* library.

$$\begin{aligned} &\mathbf{Z_{DQsym}} \\ &= \mathbf{X_{DQsym}} \times \mathbf{Y_{DQsym}} \\ &= \begin{bmatrix} 0 & 0.68{-}0.45i & -0.22{-}0.33i & -0.12{+}0.00i & \cdots \\ 0 & 0.11{-}0.07i & -0.05{-}0.16i & -0.52{+}0.81i & \cdots \\ 0 & 0.52{+}0.36i & -0.01{+}0.03i & 0.10{+}0.58i & \cdots \end{bmatrix} \\ &\quad \times \begin{bmatrix} 0 & 0.35{+}0.18i & 0.12{+}0.02i & -0.23{-}0.49i & \cdots \\ 0 & -0.56{+}0.39i & -0.12{+}0.26i & 0.01{-}0.03i & \cdots \\ 0 & -0.80{+}0.57i & 0.63{-}0.17i & 0.55{+}0.51i & \cdots \end{bmatrix} \end{aligned} \tag{34}$$

The *DQsym* output is validated against EMT simulation results obtained in MATLAB. Fig. 4 shows the three output

$$C_0 = a_0b_0 + \sum_{i=1}^{N}\left(\tfrac{1}{2}a_i^s b_i^s + \tfrac{1}{2}a_i^c b_i^c\right), \tag{27a}$$

$$C_k^s = \sum_{\substack{i+j=k \\ 1\le i,j\le N}} \tfrac{1}{2}\left(a_i^s b_j^c + a_i^c b_j^s\right) + \sum_{\substack{|i-j|=k \\ 1\le i,j\le N}} \tfrac{1}{2}\operatorname{sgn}(i-j)\left(a_i^s b_j^c - a_i^c b_j^s\right) + a_0 b_k^s + b_0 a_k^s, \tag{27b}$$

$$C_k^c = \sum_{\substack{i+j=k \\ 1\le i,j\le N}} \tfrac{1}{2}\left(a_i^c b_j^c - a_i^s b_j^s\right) + \sum_{\substack{|i-j|=k \\ 1\le i,j\le N}} \tfrac{1}{2}\left(a_i^c b_j^c + a_i^s b_j^s\right) + a_0 b_k^c + b_0 a_k^c. \tag{27c}$$

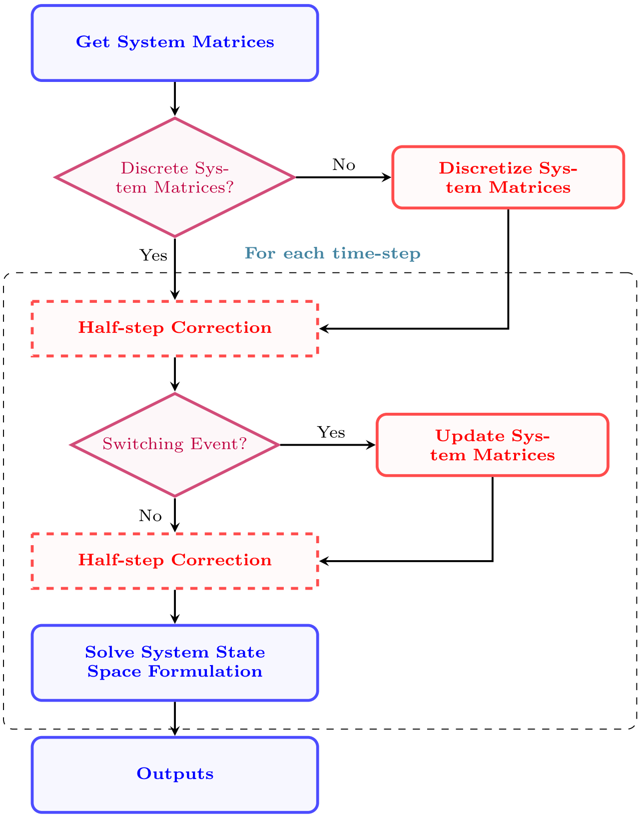


**FIGURE 2.** ***DQsym*** **state-space masked block and internal algorithm flowchart.**

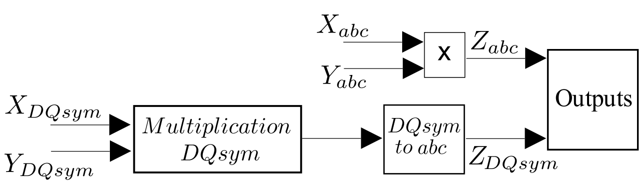


**FIGURE 3.** **Output signal $Z^{p,n,z}_{dqn}(10) = x^{p,n,z}_{dqn}(5) \cdot y^{p,n,z}_{dqn}(5)$ computed using a multiplication block from the *DQsym* library, as implemented in MATLAB/Simulink.**

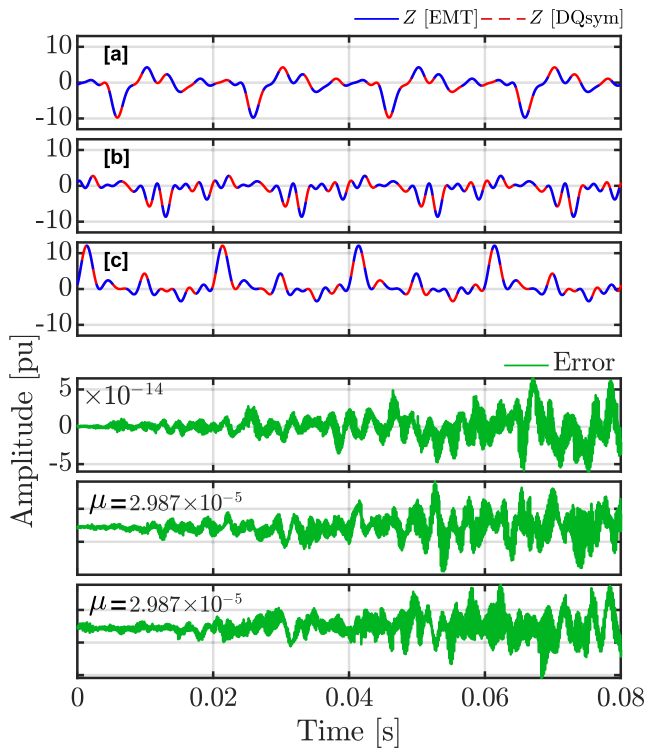


**FIGURE 4.** **Output signal $Z^{p,n,z}_{dqn}(10) = x^{p,n,z}_{dqn}(5) \cdot y^{p,n,z}_{dqn}(5)$ from the DQsym multiplication block compared with EMT results (top three subplots), and the corresponding pointwise error (bottom three subplots). The phase a error lies within $\pm 5 \times 10^{-14}$ pu; phases b and c exhibit a mean error of $\mu = 2.987 \times 10^{-5}$ pu.**

**TABLE 1.** **FFT analysis comparison: Z[EMT] vs. *Z[DQsym]*.**

| Freq. (Hz) | Comp. | Mag.$_{EMT}$ (%) | Ph.$_{EMT}$ (°) | Mag.$_{DQ}$ (%) | Ph.$_{DQ}$ (°) |
|---|---|---|---|---|---|
| 0 | DC | 114.70 | 90.0 | 114.70 | 90.0 |
| 50 | Fnd | 100.00 | 77.2 | 100.00 | 77.2 |
| 100 | h2 | 101.99 | 111.3 | 101.99 | 111.3 |
| 150 | h3 | 104.84 | 194.6 | 104.84 | 194.6 |
| 200 | h4 | 170.52 | −73.1 | 170.52 | −73.1 |
| 250 | h5 | 75.30 | −7.5 | 75.30 | −7.5 |
| 300 | h6 | 89.65 | 148.3 | 89.65 | 148.3 |
| 350 | h7 | 108.15 | 174.2 | 108.15 | 174.2 |
| 400 | h8 | 139.42 | 154.7 | 139.42 | 154.7 |
| 450 | h9 | 52.07 | 167.5 | 52.07 | 167.5 |
| 500 | h10 | 119.01 | 175.7 | 119.01 | 175.7 |

components $Z^{p,n,z}$ alongside the pointwise error between the two methods, which remains on the order of $10^{-14}$ pu throughout the simulation window, confirming that the *DQsym* multiplication block reproduces the EMT result to numerical precision. Table 1 further quantifies this agreement via an FFT analysis: the magnitude and phase of each harmonic component from DC up to the 10$^{th}$ order are identical between the EMT and *DQsym* results to the number of decimal places reported, with a total harmonic distortion of 334.95% in both cases.

### B. RLC CIRCUIT

To verify that the proposed *DQsym* formulation and its state-space implementation are correct, a simple *RLC* test circuit is used as the first validation case. The test system is a series *RL* circuit with a resistor *R* and an inductor *L*, supplying a load made of a parallel resistor *R* and a capacitor *C*. The source voltage contains harmonics up to the 5th order. The circuit is built in MATLAB/Simulink using blocks from the Specialized Power Systems (SPS) library together with the *DQsym* state-space block, as shown in Fig. 5. First, the differential equations to capture the system dynamic are written as in (35), where $\varphi \in \{a, b, c\}$.

$$L\frac{di\varphi}{dt} = v_{s,\varphi} - v_{C,\varphi} - R_{s,\varphi} i_{\varphi}, \quad C\frac{dv_{C,\varphi}}{dt} = i_{\varphi} - \frac{v_{C,\varphi}}{R_L}. \tag{35}$$

Second, rewrite the equations (35) in terms of dynamic phasors, by replacing the state variables, inputs, and time derivatives with their corresponding DPs as in (36a)

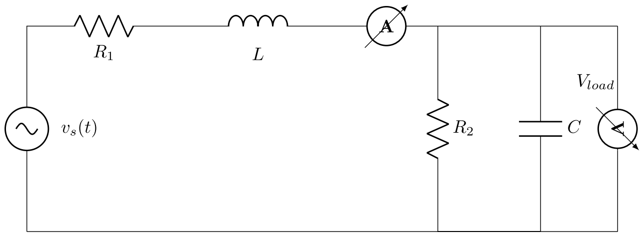


**FIGURE 5. Overview of RLC test case in both the SPS and *DQsym* library blocks.**

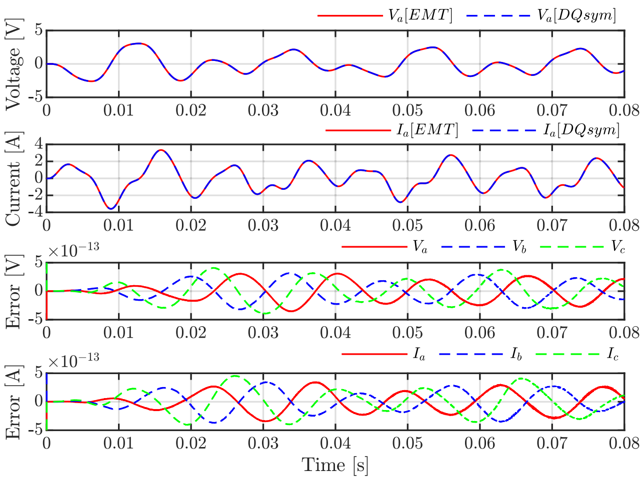


**FIGURE 6. Comparison of phase-*a* voltage and current responses of the RLC circuit obtained from EMT and *DQsym* simulations.**

and (36b),

$$L\frac{d}{dt}\langle i_\varphi\rangle_k = \langle v_{s,\varphi}\rangle_k - \langle v_{C,\varphi}\rangle_k - \big(R_{s,\varphi} + jk\omega_0 L\big)\langle i_\varphi\rangle_k \quad (36a)$$

$$C\frac{d}{dt}\langle v_{C,\varphi}\rangle_k = \langle i_\varphi\rangle_k - \left(\frac{1}{R_{L,\varphi}} + jk\omega_0 C\right)\langle v_{C,\varphi}\rangle_k \quad (36b)$$

$$\langle \vec{x}\rangle_k = \left[\langle \vec{i}_\varphi\rangle_k, \langle \vec{v}_{c,\varphi}\rangle_k\right]^T, \qquad \langle \vec{u}\rangle_k = \left[\langle \vec{v}_{s,\varphi}\rangle_k\right] \quad (36c)$$

Finally, transformations are applied to represent the RLC model in the *DQsym* frame. As in (20), the $k$th DP components are first mapped into orthogonal components and then rotated by $T_{\mathrm{Rot}}$ so that each retained harmonic is expressed in *DQ* variables. The state and input vectors are given in (37), where $j \in \{p, n, z\}$, with the states corresponding to the inductor current and capacitor voltage. Each state and input variable is complex-valued, where $\Re\{\cdot\}$ corresponds to the $d$ component and $\Im\{\cdot\}$ corresponds to the $q$ component.

$$T^{dq}_{pnz} = T_{Rot}.T_{pnz} \quad \langle \vec{x}\rangle^{dq}_k = T^{dq}_{pnz}\langle \vec{x}\rangle_k \quad \langle \vec{u}\rangle^{dq}_k = T^{dq}_{pnz}\langle \vec{u}\rangle_k$$
$$\langle \vec{x}\rangle^{dq}_k = \left[\langle \vec{i}_j\rangle^{dq}_k, \langle \vec{v}_{c,j}\rangle^{dq}_k\right]^T, \qquad \langle \vec{u}\rangle^{dq}_k = \left[\langle \vec{v}_{s,j}\rangle^{dq}_k\right] \quad (37)$$

The circuit parameters are first selected, after which the corresponding state-space matrices are formed explicitly and provided to the *DQsym* block without further adjustment.

The *DQsym* implementation closely matches the time-domain voltage response of the RLC circuit. The EMT and *DQsym* phase waveforms overlap almost exactly, with a maximum error of $5 \times 10^{-3}$, as shown in Fig. 6. In addition to waveform comparison, the frequency content is analyzed using the FFT tool in MATLAB/Simulink as illustrated in Fig. 7 and quantified in Table 2. The per-harmonic magnitudes and phases obtained from both models are identical to the number of decimal places reported, and the THD values agree exactly at 52.79% for both EMT and *DQsym*. This exact agreement is consistent with the linear, non-multiplicative structure of the RLC equations (35): since

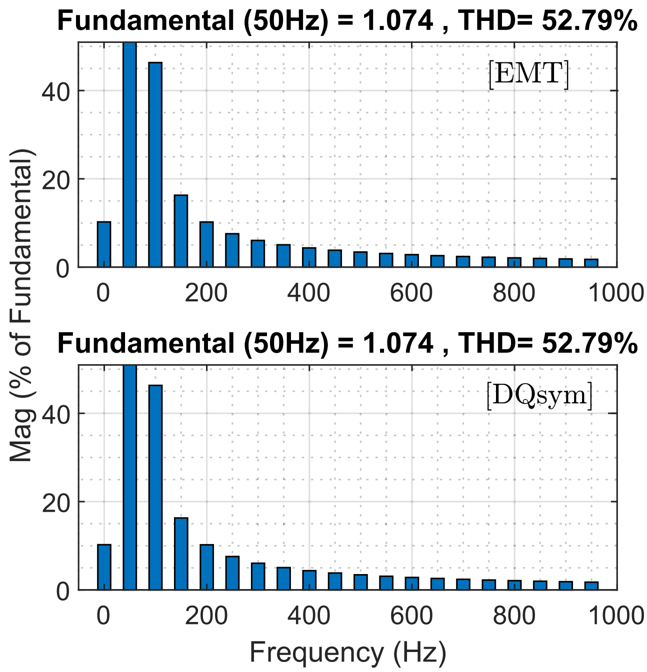


**FIGURE 7. FFT-based spectral of current measured in the RLC circuit using *DQsym* models, with corresponding Total Harmonic Distortion (THD) values confirming consistency in harmonic content with EMT.**

**TABLE 2. FFT analysis comparison: EMT vs. *DQsym*–RLC circuit.**

| Freq. (Hz) | Comp. | $\mathrm{Mag}_{\mathrm{EMT}}$ (%) | $\mathrm{Ph}_{\mathrm{EMT}}$ (°) | $\mathrm{Mag}_{\mathrm{DQ}}$ (%) | $\mathrm{Ph}_{\mathrm{DQ}}$ (°) |
|---|---|---|---|---|---|
| 0 | DC | 10.24 | 90.0 | 10.24 | 90.0 |
| 50 | Fnd | 100.00 | 95.1 | 100.00 | 95.1 |
| 100 | h2 | 46.33 | 227.2 | 46.33 | 227.2 |
| 150 | h3 | 16.29 | 210.3 | 16.29 | 210.3 |
| 200 | h4 | 10.22 | 203.1 | 10.22 | 203.1 |
| 250 | h5 | 7.56 | 198.9 | 7.56 | 198.9 |
| 300 | h6 | 6.04 | 196.1 | 6.04 | 196.1 |
| 350 | h7 | 5.05 | 194.2 | 5.05 | 194.2 |
| 400 | h8 | 4.35 | 192.8 | 4.35 | 192.8 |
| 450 | h9 | 3.83 | 191.7 | 3.83 | 191.7 |
| 500 | h10 | 3.42 | 190.9 | 3.42 | 190.9 |
| 550 | h11 | 3.09 | 190.2 | 3.09 | 190.2 |
| 600 | h12 | 2.82 | 189.7 | 2.82 | 189.7 |
| 650 | h13 | 2.59 | 189.3 | 2.59 | 189.3 |
| 700 | h14 | 2.40 | 189.0 | 2.40 | 189.0 |
| 750 | h15 | 2.24 | 188.8 | 2.24 | 188.8 |
| 800 | h16 | 2.09 | 188.6 | 2.09 | 188.6 |
| 850 | h17 | 1.97 | 188.4 | 1.97 | 188.4 |
| 900 | h18 | 1.86 | 188.3 | 1.86 | 188.3 |
| 950 | h19 | 1.76 | 188.2 | 1.76 | 188.2 |
| THD | | 52.79% | — | 52.79% | — |

no harmonic convolution is involved, no per-step truncation error is introduced, and the *DQsym* state-space integration reproduces the EMT result to numerical precision across all retained harmonic orders.

### C. HYBRID AC/DC IEEE-9 BUS NETWORK

To verify that the proposed *DQsym* formulation and its state-space implementation can simulate hybrid AC/DC power networks, a modified Hybrid AC/DC IEEE 9-bus system is considered. The generators in the original IEEE 9-bus network are replaced with ideal AC voltage sources. As a result, mechanical dynamics such as rotor angle and speed are not included, and the system is treated purely as an electrical network governed by Kirchhoff's voltage and current laws.

The system is further modified by replacing the transmission line between Bus 1 and Bus 2 with a point-to-point HVDC link based on Modular Multilevel Converters (MMCs). This introduces additional electrical components, including converter arm inductors, arm capacitor voltages, and the DC-link circuit. These elements add new differential equations to the network model. Consequently, the state vector is expanded to include both AC network and HVDC converter states, and the system matrices are updated to capture the interaction between the AC system and the HVDC link.

To obtain the state-space representation, the same procedure used for the RLC test case is followed. The circuit equations are first written in the time domain, and the inductor currents and capacitor voltages are selected as state variables. The required transformations are then applied to express the complete network model in *DQsym* coordinates. Given its importance, only the MMC modelling will be explained in detail.

By assembling all equations into a matrix, the overall system is written in standard state-space form. Since the generators are modeled as fixed-voltage sources, the state matrix captures only the electrical behavior of the network and does not include the mechanical dynamics of the generators.

For all *DQsym* simulations of the IEEE-9 bus MMC-HVDC, the harmonic series is truncated to order $N = 5$, retaining the DC component and the first five harmonic orders for each sequence ($p$, $n$, $z$). Higher-order harmonic content present in the EMT reference but outside this retained set is not represented in the *DQsym* state vector, and its effect on the THD comparison is discussed in Section IV-E.

### D. MMC IN DQSYM FRAME

An MMC phase leg consists of an upper and a lower arm connected between the DC bus and the AC terminal. Each arm contains a series inductor $L_{arm}$, resistance $R_{arm}$, and an equivalent capacitor representing the sum of the submodule capacitors. The AC side is connected to the network through an equivalent filter impedance. To simplify the model, the arm average representation is used. In this approach, each arm is described by an equivalent capacitor voltage and a controlled voltage source defined by the modulation signal. This captures the main electrical behavior without modelling individual submodules.

The modulated arm voltages and currents are as in (38), $\varphi \in \{a, b, c\}$:

$$\begin{aligned} v^u_{m\varphi} &= m^u_\varphi v^u_{C\varphi}, \quad v^l_{m\varphi} = m^l_\varphi v^l_{C\varphi}, \\ i^u_{m\varphi} &= m^u_\varphi i^u_\varphi, \quad i^l_{m\varphi} = m^l_\varphi i^l_\varphi, \end{aligned} \tag{38}$$

where $m^u_\varphi$ and $m^l_\varphi$ are the upper and lower modulation indices. For analysis, it is convenient to use sum and difference variables:

$$\begin{aligned} i^\Delta_\varphi &= i^u_\varphi - i^l_\varphi, \quad i^\Sigma_\varphi = \tfrac{1}{2}(i^u_\varphi + i^l_\varphi), \\ v^\Delta_{C\varphi} &= v^u_{C\varphi} - v^l_{C\varphi}, \quad v^\Sigma_{C\varphi} = \tfrac{1}{2}(v^u_{C\varphi} + v^l_{C\varphi}). \end{aligned} \tag{39}$$

Here, $i^\Delta_j$ is the grid current and $i^\Sigma_j$ is the circulating current inside the converter. $\vec{1} \triangleq [1 \ 1 \ 1]^T$ and $\odot$ denotes element-wise multiplication of vectors. Using these definitions, the AC-side current (40a), circulating current (40b), and capacitor voltage dynamics (40c) are as follows. These equations define the averaged nonlinear MMC model.

$$L^{ac}_{eq} \frac{d\vec{i}^\Delta_\varphi}{dt} = \vec{v}^g_\varphi - R^{ac}_{eq}\vec{i}^\Delta_\varphi - \vec{v}^\Delta_{m\varphi}, \tag{40a}$$

$$L_{arm} \frac{d\vec{i}^\Sigma_\varphi}{dt} = \frac{v_{dc}}{2}\vec{1} - R_{arm}\vec{i}^\Sigma_\varphi - \vec{v}^\Sigma_{m\varphi}, \tag{40b}$$

$$\begin{aligned} 2C_{arm} \frac{d\vec{v}^\Sigma_{C,\varphi}}{dt} &= \tfrac{1}{2}\vec{m}^\Delta_\varphi \odot \vec{i}^\Delta_\varphi + \vec{m}^\Sigma_\varphi \odot \vec{i}^\Sigma_\varphi, \\ 2C_{arm} \frac{d\vec{v}^\Delta_{C,\varphi}}{dt} &= \tfrac{1}{2}\vec{m}^\Sigma_\varphi \odot \vec{i}^\Delta_\varphi + \vec{m}^\Delta_\varphi \odot \vec{i}^\Sigma_\varphi. \end{aligned} \tag{40c}$$

The above equations are rewritten in dynamic phasor form by replacing each variable with its harmonic component $\langle\cdot\rangle_k$. The state vector and the input vector are given in (41a), and then transformed to the *DQsym* frame following the procedure in (20), yielding (41b) where $j \in \{p, n, z\}$ and each variable is complex-valued.

$$\begin{aligned} \langle\vec{x}\rangle_k &= [\langle\vec{i}^\Delta_\varphi\rangle_k \quad \langle\vec{i}^\Sigma_\varphi\rangle_k \quad \langle\vec{v}^\Delta_{C,\varphi}\rangle_k \quad \langle\vec{v}^\Sigma_{C,\varphi}\rangle_k]^T, \\ \langle\vec{u}\rangle_k &= [\langle\vec{v}^g_\varphi\rangle_k \quad \langle\vec{v}^\Delta_{m,\varphi}\rangle_k \quad \langle\vec{v}^\Sigma_{m,\varphi}\rangle_k \quad \langle v_{dc,\varphi}\rangle_k]^T, \end{aligned} \tag{41a}$$

$$\begin{aligned} \langle\vec{x}\rangle^{dq}_k &= [\langle\vec{i}^\Delta_j\rangle^{dq}_k \quad \langle\vec{i}^\Sigma_j\rangle^{dq}_k \quad \langle\vec{v}^\Delta_{C,j}\rangle^{dq}_k \quad \langle\vec{v}^\Sigma_{C,j}\rangle^{dq}_k]^T, \\ \langle\vec{u}\rangle^{dq}_k &= [\langle\vec{v}^g_j\rangle^{dq}_k \quad \langle\vec{v}^{`\Delta}_{m,j}\rangle^{dq}_k \quad \langle\vec{v}^\Sigma_{m,j}\rangle^{dq}_k \quad \langle v_{dc,j}\rangle^{dq}_k]^T \end{aligned} \tag{41b}$$

The MMC station controller generates control signals at the fundamental frequency using a phase-locked loop (PLL) and includes second-harmonic control to reduce internal circulating currents. The control system contains an active power controller, a reactive power controller, and a current controller. All controllers are implemented as PI controllers. Since both the controller and the system model use the same $dq$ representation, no extra coordinate transformations are required. Only the positive-sequence fundamental-frequency components are needed, which can be directly obtained from the measured voltages and currents.

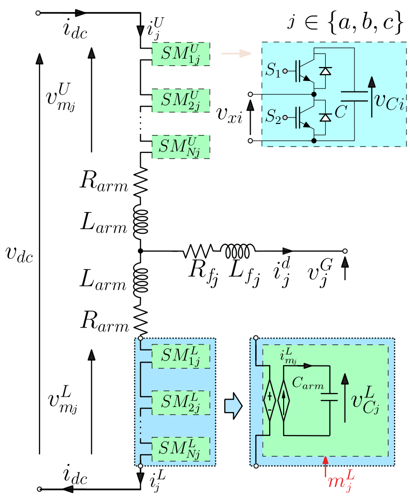

FIGURE 8. **Circuit diagram of the MMC converter showing the grid current, positive and negative arm current directions.**

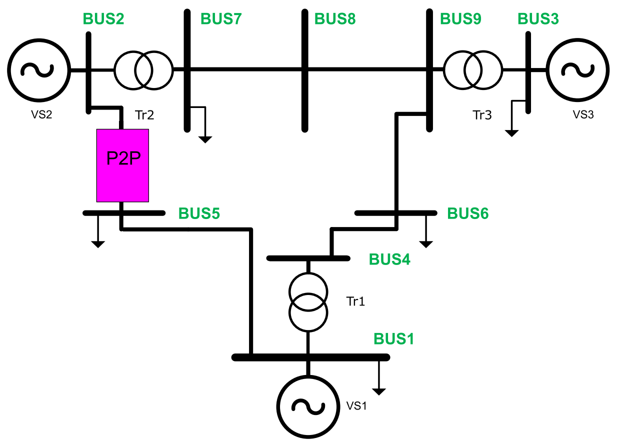


FIGURE 9. **A diagram of the IEEE 9-bus system extended with a point-to-point HVDC system, MMC converters connected between bus 1 and bus 5.**

The overall system model is obtained by combining the individual state-space representations of the network and the point-to-point HVDC MMC transmission system into a single, unified set of equations.

### *E. COMPARISON OF DQSYM SIMULATIONS AND EMT SIMULATIONS*

Figs. 10–13 compare the EMT reference simulation with the corresponding *DQsym* simulation. Both models are implemented in MATLAB/Simulink: the EMT model using the SPS library blocks and the reduced-order model using the *DQsym* library.

Figure 10 presents the Bus 1 and Bus 2 currents together with the corresponding phase errors between EMT and *DQsym*. Prior to the active power step at $t \approx 5.0$ s, the error remains within approximately 0.005 kA (5 A), corresponding to about 0.35% (0.0035 p.u.) of the base current ($I_{\text{base}} \approx 1.44$ kA). Immediately after the step, the maximum transient deviation reaches approximately 0.5 kA, i.e., about 34.7% (0.347 p.u.). This transient error decays rapidly, and the post-transient deviation settles to less than 0.02 kA (20 A), corresponding to about 1.4% (0.014 p.u.).

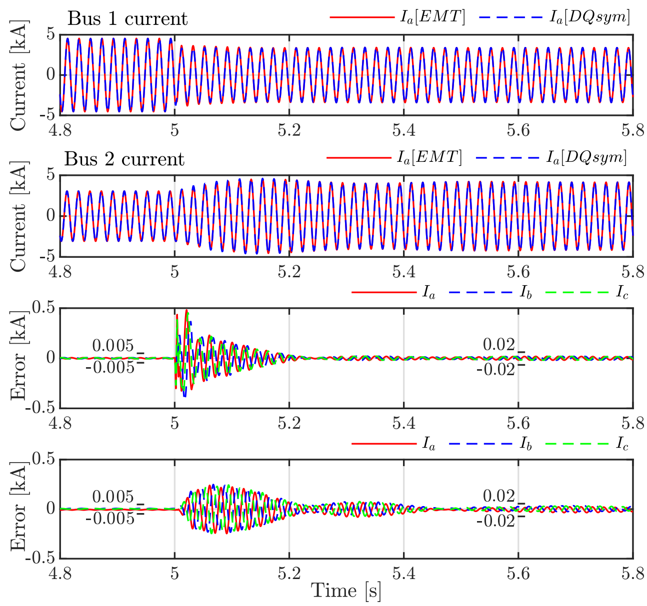

FIGURE 10. **Comparison of bus 1 and bus 2 currents and the corresponding error between all phases obtained from EMT and *DQsym* simulations.**

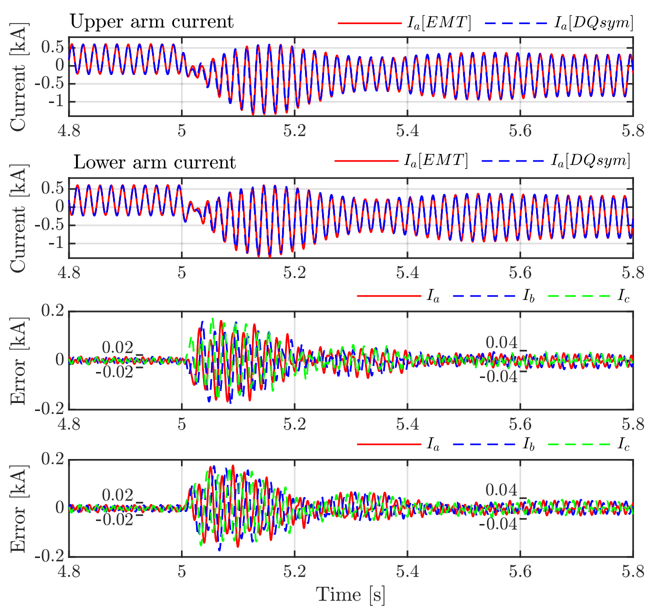

FIGURE 11. **Comparison of phases-*a* upper and lower arm currents for MMC 1 in response to a change in active power, and the corresponding error between all phases. obtained from EMT and *DQsym* simulations.**

Figure 11 compares the phase-*a* upper and lower arm currents of MMC 1 (converter station) and their corresponding errors. Before the step change, the error is within approximately 0.02 kA (20 A), i.e., about 1.4% (0.014 p.u.).

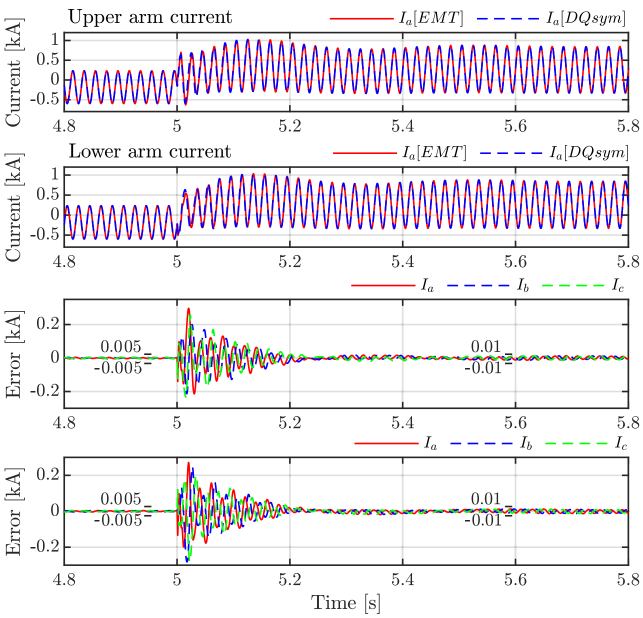


**FIGURE 12.** **The error between phases-*abc* upper and lower arms currents for MMC 2 in response to a change in active power, and the corresponding error between all phases. obtained from EMT and *DQsym* simulations.**

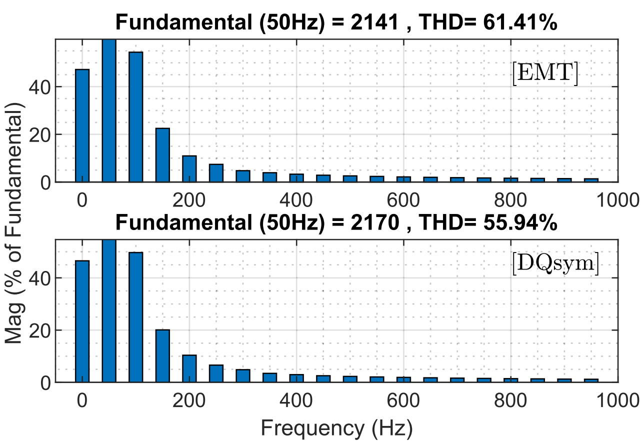


**FIGURE 13.** **FFT-based spectral MMC 1 upper arm currents from *DQsym* blocks, with corresponding Total Harmonic Distortion (THD) values confirming consistency in harmonic content with EMT.**

Following the active power step, the maximum transient deviation reaches approximately 0.2 kA, corresponding to about 13.9% (0.139 p.u.) of the base current. The error then decreases and remains below 0.04 kA (40 A), i.e., about 2.8% (0.028 p.u.), during the post-transient period. The upper-and lower-arm responses remain balanced, and the error profiles are comparable across phases.

Figure 12 shows the phase-*abc* upper and lower arm currents for MMC 2 (inverter station) and the corresponding error between EMT and *DQsym*. Before the step, the deviation is within approximately 0.005 kA (5 A), or 0.35% (0.0035 p.u.). After the active power change, the maximum

**TABLE 3.** **MMC station data.**

| Parameter & Description | Value |
|---|---|
| $S_b$: Base power | 1000 MVA |
| $R_{\text{arm}}$: Arm resistance | 166 m$\Omega$ |
| $R_{\text{G}}$: Equivalent transformer resistance | 400 m$\Omega$ |
| $R_{\text{L}}$: Equivalent load resistance | 240 $\Omega$ |
| $L_{\text{arm}}$: Arm inductance | 52.94 mH |
| $L_{\text{G}}$: Equivalent transformer inductance | 52 mH |
| $C$: Submodule capacitance | 1.758 mF |
| $N_{sm}$: Number of submodules | 216 |
| $\omega_g$: Fundamental grid frequency | $2\pi \cdot 50$ rad/s |
| $V_{\text{DC}}$: Rated pole-to-pole DC voltage | 640 kV |
| $V_{\text{PCC}}$: Rated line-to-line PCC voltage | 400 kV |
| $V_{\text{sec}}$: Rated transformer secondary voltage, line-to-line | 333 kV |
| $K_p^{i,\text{out}}$: Output current controller proportional gain | 0.6 A/V |
| $K_i^{i,\text{out}}$: Output current controller integral gain | 6 A/(V·s) |
| $K_p^{Q}$: Reactive power controller proportional gain | 0.167 A/V |
| $K_i^{Q}$: Reactive power controller integral gain | 1 A/(V·s) |
| $K_p^{i,z}$: Zero-sequence circulating current controller proportional gain | 1 A/V |
| $K_i^{i,z}$: Zero-sequence circulating current controller integral gain | 5 A/(V·s) |

**TABLE 4.** **FFT analysis comparison: EMT vs. *DQsym*–MMC 1 upper arm current.**

| Freq. (Hz) | Comp. | $\text{Mag.}_{\text{EMT}}$ (%) | $\text{Ph.}_{\text{EMT}}$ ($^\circ$) | $\text{Mag.}_{\text{DQ}}$ (%) | $\text{Ph.}_{\text{DQ}}$ ($^\circ$) |
|---|---|---|---|---|---|
| 0 | DC | 47.19 | 270.0 | 46.52 | 270.0 |
| 50 | Fnd | 100.00 | 147.0 | 100.00 | 145.8 |
| 100 | h2 | 54.44 | −51.1 | 49.69 | −51.2 |
| 150 | h3 | 22.50 | −21.9 | 20.08 | −28.6 |
| 200 | h4 | 10.95 | 40.9 | 10.39 | 41.8 |
| 250 | h5 | 7.41 | −5.3 | 6.61 | −0.9 |
| 300 | h6 | 4.76 | −9.9 | 4.85 | −13.7 |
| 350 | h7 | 3.91 | −5.2 | 7.45 | −7.6 |
| 400 | h8 | 3.29 | −3.6 | 2.96 | −5.2 |
| 450 | h9 | 2.87 | −1.7 | 2.54 | −3.1 |
| 500 | h10 | 2.58 | −0.1 | 2.28 | −1.2 |
| 550 | h11 | 2.36 | 0.3 | 2.08 | −0.1 |
| 600 | h12 | 2.15 | 0.6 | 1.91 | 0.1 |
| 650 | h13 | 1.99 | 1.1 | 1.75 | 0.6 |
| 700 | h14 | 1.84 | 1.4 | 1.63 | 1.1 |
| 750 | h15 | 1.72 | 1.8 | 1.52 | 1.3 |
| 800 | h16 | 1.61 | 2.0 | 1.42 | 1.7 |
| 850 | h17 | 1.51 | 2.2 | 1.34 | 1.9 |
| 900 | h18 | 1.43 | 2.4 | 1.27 | 2.1 |
| 950 | h19 | 1.35 | 2.6 | 1.20 | 2.3 |
| THD | | 61.41% | — | 55.94% | — |

transient deviation reaches approximately 0.2 kA (about 13.9%, or 0.139 p.u.), and subsequently decays to less than 0.01 kA (10 A), corresponding to about 0.69% (0.0069 p.u.). The error magnitudes are consistent across phases and between upper and lower arms, confirming strong agreement once the transient subsides.

Figure 13 compares the FFT spectra of the MMC 1 arm currents, with per-harmonic magnitudes and phases reported in Table 4. The fundamental (50 Hz) component is 2141 in EMT and 2170 in *DQsym*, a difference of 29 (approximately 1.35%). The total harmonic distortion (THD) is 61.41% in EMT and 55.94% in *DQsym*, corresponding to a difference of 5.47 percentage points. Two distinct mechanisms contribute to this discrepancy.

The first is harmonic truncation. The *DQsym* simulation retains harmonics up to order $N = 5$, so any energy that the EMT model places in harmonics above the 5th order is structurally absent from the *DQsym* reconstruction. Since THD aggregates all harmonic content above the fundamental, this absence biases the *DQsym* THD low relative to EMT by

**TABLE 5. Computational performance comparison: EMT vs. *DQsym*.**

| Test Case | States | Step (s) | EMT (s) | DQsym MATLAB (s) | DQsym C++ (s) |
|---|---|---|---|---|---|
| RLC Circuit | 6 | $2 \times 10^{-5}$ | 2.583 | 16.714 | 0.083 |
| Single-Station MMC | 18 | $2 \times 10^{-5}$ | 19.424 | 91.000 | 19.241 |
| Point-to-Point HVDC | 34 | $2 \times 10^{-5}$ | 16.200 | 217.806 | — |

construction, and is not indicative of inaccuracy within the retained harmonic orders.

The second mechanism affects the retained harmonics themselves and is specific to components with multiplicative dynamics such as the MMC. The capacitor voltage dynamics (Eq. (40c)) involve a convolution–integration–convolution chain at each time step. The modulation and current signals are first multiplied via harmonic convolution to update the capacitor voltage states $\langle \vec{v}^{\Sigma}_{C,\phi} \rangle_k$ and $\langle \vec{v}^{\Delta}_{C,\phi} \rangle_k$, which are then integrated, and the updated capacitor voltages are subsequently multiplied again with the modulation signals to compute the arm voltages $v^{u}_{m\phi}$ and $v^{l}_{m\phi}$. At each convolution step, cross-terms above order $N = 5$ are discarded and this per-step truncation error $\epsilon$ is integrated into the capacitor voltage states and recirculates through the closed-loop controller at every subsequent time step. Over $5 \times 10^5$ integration steps ($\Delta t = 2 \times 10^{-5}$ s, $t_{\text{end}} = 10$ s), these errors compound and introduce a systematic bias into the retained harmonic magnitudes. This explains the discrepancies observed in h2 (54.44% EMT vs. 49.69% *DQsym*) and h3 (22.50% vs. 20.08%), and is consistent with the h7 result (3.91% EMT vs. 7.45% *DQsym*), where accumulated truncation error aliases back into the 7th harmonic across the integration window. This mechanism is absent in the static multiplication validation (Section IV-A), where inputs are exactly band-limited to order $N$ and the multiplication result is reproduced to numerical precision ($\sim 10^{-14}$ pu), and in the RLC case (Section IV-B), where no multiplicative dynamics are present.

Despite these discrepancies, the per-harmonic phase agreement reported in Table 4 is strong across all retained orders, and the dominant harmonic components occur at consistent frequencies in both models, confirming that *DQsym* correctly tracks the harmonic structure of the system within the retained set. Both mechanisms reflect the accuracy-versus-truncation-order trade-off inherent to the proposed framework.

### F. COMPUTATIONAL PERFORMANCE

Table 5 summarizes the computational performance of the proposed *DQsym* framework across the three test cases considered in this work, reporting the number of harmonic-domain states, the simulation time step, and the wall-clock execution time for a 10-second simulation run. All simulations were carried out on a Dell Latitude 7440 laptop equipped with a 13th Gen Intel Core i7-1365U processor (1.80 GHz) and 16.0 GB of RAM, running Windows 11. The *DQsym* library is developed and tested using MATLAB R2024a with core functionality relying on Simulink and Simscape Electrical, with additional dependencies on the Signal Processing Toolbox and DSP System Toolbox. Results are compared against an equivalent EMT model implemented in MATLAB/Simulink, and where available, against the C++ reimplementation of the *DQsym* framework.

The MATLAB-based *DQsym* library [19] is consistently slower than the EMT reference across all three test cases. For the RLC circuit, the *DQsym* MATLAB implementation requires 16.714 s compared to 2.583 s for EMT, a slowdown of approximately 6.5×. For the single-station MMC, execution time increases from 19.424 s (EMT) to 91.000 s (*DQsym* MATLAB), and for the point-to-point HVDC case the *DQsym* MATLAB library requires 217.806 s against 16.200 s for EMT. This consistent overhead reflects a known limitation of the current MATLAB-based implementation. As the number of harmonic-domain states grows, the matrix assembly and algebraic operations incur significant interpreter overhead that offsets any reduction in integration steps.

The C++ reimplementation substantially mitigates this overhead. For the RLC circuit, the C++ implementation executes in 0.083 s, a speedup of approximately 31× over the EMT reference. For the single-station MMC, the C++ implementation reduces execution time to 19.241 s, approaching the EMT reference of 19.424 s. These results confirm that the interpreter overhead is the dominant bottleneck in the MATLAB-based *DQsym* library rather than an intrinsic limitation of the *DQsym* framework itself. Extending the C++ implementation to the point-to-point HVDC case and to larger multi-terminal systems is a primary objective of future development.

The time step used in these simulations ($\Delta t = 2 \times 10^{-5}$ s) matches that of the EMT reference, chosen to ensure a fair comparison of accuracy rather than computational speed. The primary objective of *DQsym* is not to achieve faster simulation through a larger time step, but to provide a structured harmonic-domain state-space representation that supports systematic network assembly and is compatible with eigenvalue-based stability analysis. Computational performance gains through larger admissible time steps are expected as the framework matures and will be explored in future work.

## V. CONCLUSION

This paper presented the *DQsym* simulation framework for harmonic-domain modelling of IBR-dominated power systems. The central contribution is a set of explicit mathematical rules governing dynamic phasor operations in the *DQsym* frame. Specifically, a harmonic convolution theorem for multiplication of truncated Fourier series, a term-by-term integration rule that introduces cross-coupling between the $d$ and $q$ components, and element-wise summation that requires no additional transformation were derived and implemented in state-space form. Together, these rules enable systematic and repeatable assembly of interconnected AC/DC network models from modular building blocks.

The framework combines these operations with multiple rotating $dq$ reference frames and positive-, negative-, and zero-sequence decomposition to represent fundamental and selected harmonic dynamics in a unified state-space structure. The approach was validated through benchmark harmonic interaction studies and an IEEE 9-bus system extended with MMC-based HVDC transmission. The results showed close agreement with EMT simulations for both fundamental and overall harmonic profiles. The observed THD discrepancy was attributed to harmonic truncation at order $N = 5$ and accumulated convolution truncation error in the closed-loop MMC dynamics, both of which reflect the accuracy-versus-truncation-order trade-off inherent to the framework rather than inaccuracy within the retained harmonic set.

The framework preserves a state-space structure, providing a foundation for future stability and control analysis. Future work will focus on extending the approach to multi-converter and large-scale hybrid AC/DC networks, validating the framework under unbalanced operating conditions using the positive-, negative-, and zero-sequence decomposition already embedded in the *DQsym* transformation, and exploring its application to system-level dynamic assessment.

## APPENDIX

*Proof:* The validity of the coefficient expressions in (27) can be established using mathematical induction on the harmonic order $N$. Let us check the correctness of the coefficient for:

### A. BASE CASE N = 0

For constant signals $x(t) = a_0$, and $y(t) = b_0$, the product is $z(t) = a_0 b_0$, which implies

$$C_0 = a_0 b_0, \quad C_k^s = 0, \quad C_k^c = 0.$$

Thus, (27) holds for $N = 0$.

### B. BASE CASE N = 1

For first-order expansions $x(t) = a_0 + a_1^s \sin(\omega t) + a_1^c \cos(\omega t)$, and $y(t) = b_0 + b_1^s \sin(\omega t) + b_1^c \cos(\omega t)$, their product is

$$\begin{aligned} z(t) = x(t)y(t) &= a_0 b_0 + a_0 b_1^s \sin(\omega t) + a_0 b_1^c \cos(\omega t) \\ &+ b_0 a_1^s \sin(\omega t) + b_0 a_1^c \cos(\omega t) + a_1^s b_1^s \sin^2(\omega t) \\ &+ a_1^c b_1^c \cos^2(\omega t) + (a_1^s b_1^c + a_1^c b_1^s) \sin(\omega t)\cos(\omega t). \end{aligned}$$

Using trigonometric identities, we group the terms as

$$\begin{aligned} z(t) = &\underbrace{\left(a_0 b_0 + \tfrac{1}{2} a_1^s b_1^s + \tfrac{1}{2} a_1^c b_1^c\right)}_{C_0} \\ &+ \underbrace{(a_1^s b_0 + a_0 b_1^s)}_{C_1^s} \sin(\omega t) + \underbrace{(a_1^c b_0 + a_0 b_1^c)}_{C_1^c} \cos(\omega t) \\ &+ \underbrace{\frac{1}{2}(a_1^s b_1^c + a_1^c b_1^s)}_{C_2^s} \sin(2\omega t) \\ &+ \underbrace{\frac{1}{2}(a_1^c b_1^c - a_1^s b_1^s)}_{C_2^c} \cos(2\omega t), \end{aligned}$$

where the coefficients are consistent with the structure given in (27). Thus, the case $N = 1$ is verified.

### C. INDUCTION STEP

Assume that (27) holds for Fourier series truncated at order $N$:

$$x'(t) = a_0 + \sum_{i=1}^{N} \left(a_i^s \sin(i\omega t) + a_i^c \cos(i\omega t)\right), \tag{42}$$

$$y'(t) = b_0 + \sum_{j=1}^{N} \left(b_j^s \sin(j\omega t) + b_j^c \cos(j\omega t)\right), \tag{43}$$

with $z'(t) = x'(t)y'(t)$ satisfies the equation (27), denoted with $C_0'$, $C_k^{s\prime}$ and $C_k^{c\prime}$, for $k \in \{1, \ldots 2N\}$, respectively.

Now we have to show that it is valied for $N + 1$, so we extend $x(t)$ and $y(t)$ with the $(N + 1)$-th harmonics:

$$\begin{aligned} x(t) &= x'(t) + \underbrace{a_{N+1}^s \sin((N+1)\omega t) + a_{N+1}^c \cos((N+1)\omega t)}_{x^{(N+1)}(t)}, \\ y(t) &= y'(t) + \underbrace{b_{N+1}^s \sin((N+1)\omega t) + b_{N+1}^c \cos((N+1)\omega t)}_{y^{(N+1)}(t)} \end{aligned} \tag{44}$$

The product expands as

$$\begin{aligned} z(t) = x(t)y(t) &= x'(t)y'(t) + x'(t)\, y^{(N+1)}(t) \\ &+ y'(t)x^{(N+1)}(t) + x^{(N+1)}(t)y^{(N+1)}(t). \end{aligned}$$

The first and last terms yield valid Fourier series with harmonics up to order $2N$ and $2N + 2$. Thus, the term $C_0$ is only influenced by $x'(t)y'(t)$ and $x^{(N+1)}(t)y^{(N+1)}(t)$, and equal to:

$$\begin{aligned} C_0 &= C_0' + \frac{1}{2}(a_{N+1}^s b_{N+1}^s + a_{N+1}^c b_{N+1}^c) \\ &= a_0 b_0 + \sum_{i=1}^{N+1} \left(\tfrac{1}{2} a_i^s b_i^s + \tfrac{1}{2} a_i^c b_i^c\right), \end{aligned}$$

and corresponds to the equation (27a).

The multiplication cross-terms introduce frequencies of the form $j = i \pm (N + 1)$, where $1 \le i \le N$, generating harmonics up to $(2N + 1)\omega$. Namely, we obtain that:

$$\begin{aligned} &x' y^{(N+1)} \\ &= a_0 b_{N+1}^s \sin((N+1)\omega t) + a_0 b_{N+1}^c \cos((N+1)\omega t) \\ &\sum_{i=1}^{N} \Bigg( \frac{1}{2}(a_i^c b_{N+1}^c - a_i^s b_{N+1}^s) \cos((N+1+i)\omega t) \\ &+ \frac{1}{2}(a_i^c b_{N+1}^c + a_i^s b_{N+1}^s) \cos((N+1-i)\omega t) \\ &+ \frac{1}{2}(a_i^c b_{N+1}^s + a_i^s b_{N+1}^c) \sin((N+1+i)\omega t) \\ &+ \frac{1}{2}(a_i^c b_{N+1}^s - a_i^s b_{N+1}^c) \sin((N+1-i)\omega t) \Bigg), \end{aligned}$$

and

$$
\begin{aligned}
&y' x^{(N+1)} \\
&= b_0 a^s_{N+1} \sin((N+1)\omega t) + b_0 a^c_{N+1} \cos((N+1)\omega t) \\
&\quad \sum_{i=1}^{N} \Bigg( \frac{1}{2}(b^c_i a^c_{N+1} - b^s_i a^s_{N+1}) \cos((N+1+i)\omega t) \\
&\quad + \frac{1}{2}(b^c_i a^c_{N+1} + b^s_i a^s_{N+1}) \cos((N+1-i)\omega t) \\
&\quad + \frac{1}{2}(b^c_i a^s_{N+1} + b^s_i a^c_{N+1}) \sin((N+1+i)\omega t) \\
&\quad + \frac{1}{2}(b^c_i a^s_{N+1} - b^s_i a^c_{N+1}) \sin((N+1-i)\omega t) \Bigg),
\end{aligned}
$$

and thus, they add spectral components to $C^{s,k}_{N+1\pm i} = C^{s,k}_j$. For

$$
\begin{aligned}
&C^s_{N+1\pm i} \\
&= C^{s\prime}_j + \frac{1}{2}(a^c_i b^s_{N+1} + b^c_i a^s_{N+1} \pm a^s_i b^c_{N+1} \pm b^s_i a^c_{N+1}), \\
&C^c_{N+1\pm i} \\
&= C^{c\prime}_j + \frac{1}{2}(a^c_i b^c_{N+1} + b^c_i a^c_{N+1} \mp a^s_i b^s_{N+1} \mp b^s_i a^s_{N+1}),
\end{aligned}
$$

which together corresponds to the format as in equation (27b) and equation (27c).

At $k = N+1$, $C^s_{N+1} = {C^s_{N+1}}' + a_0 b^s_{N+1} + b_0 a^s_{N+1}$ and $C^c_{N+1} = {C^c_{N+1}}' + a_0 b^c_{N+1} + b_0 a^c_{N+1}$ also correspond equation (27b) and equation (27c).

Furthermore, the coefficients for when $k = 2(N+1)$ only depend on $x^{(N+1)}(t) y^{(N+1)}(t)$ and are equal to:

$$
\begin{aligned}
C^s_{2(N+1)} &= \frac{1}{2}(a^s_{N+1} b^c_{N+1} + a^c_{N+1} b^s_{N+1}), \\
C^c_{2(N+1)} &= \frac{1}{2}(a^c_{N+1} b^c_{N+1} - a^s_{N+1} b^s_{N+1}),
\end{aligned}
$$

and also satisfies equations (27b) and (27c) for $k = 2(N+1)$. By induction, the coefficient expressions in (27) hold for all $N \geq 0$, which completes the proof. ■

## REFERENCES


[1] J. D. Lara, R. Henriquez-Auba, D. Ramasubramanian, S. Dhople, D. S. Callaway, and S. Sanders, "Revisiting power systems time-domain simulation methods and models," *IEEE Trans. Power Syst.*, vol. 39, no. 2, pp. 2421–2437, Mar. 2024.

[2] C. Shah et al., "Review of dynamic and transient modeling of power electronic converters for converter dominated power systems," *IEEE Access*, vol. 9, pp. 82094–82117, 2021.

[3] L. B. Larumbe, "Harmonic stability and distortion in offshore wind farms," *Ph.D. dissertation, Delft Univ. Technol.*, Delft, The Netherlands, 2024.

[4] V. Sewdien, "Sub synchronous oscillations in modern transmission grids: Design and validation of novel concepts for mitigating adverse dfig-ssr interactions," *Ph.D. dissertation, Delft Univ.Technol.*, Delft, The Netherlands, 2021.

[5] Ö. C. Sakinci and J. Beerten, "Modeling of the modular multilevel converter using dynamic phasors: Reduced-order models for small-signal stability analysis," Ph.D. dissertation, KU Leuven Univ., Leuven, Belgium, 2022.

[6] Ö. C. Sakinci, A. Lekić, and J. Beerten, "Generalized impedance-based AC/DC power system modeling for harmonic stability analysis," *Int. J. Electr. Power Energy Syst.*, vol. 143, Dec. 2022, Art. no. 108456.

[7] H. Fang, H. Xiang, S. Li, Y. Xin, J. Zhou, and Y. Wang, "Dynamic phasor modeling of MMC-HVDC systems," in *Proc. IEEE 5th Int. Conf. Inf. Syst. Comput. Aided Educ. (ICISCAE)*, Sep. 2022, pp. 988–995.

[8] J. Dinkelbach, M. Moraga, and A. Monti, "Reduced-order synchronous generator modelling for real- time simulation using shifted frequency analysis," in *Proc. Open Source Modeling Simulation Energy Syst. (OSMSES)*, Mar. 2023, pp. 1–6.

[9] A. M. Stankovic, S. R. Sanders, and T. Aydin, "Dynamic phasors in modeling and analysis of unbalanced polyphase AC machines," *IEEE Trans. Energy Convers.*, vol. 17, no. 1, pp. 107–113, Mar. 2002.

[10] P. De Rua, Ö. C. Sakinci, and J. Beerten, "Comparative study of dynamic phasor and harmonic state-space modeling for small-signal stability analysis," *Electr. Power Syst. Res.*, vol. 189, Dec. 2020, Art. no. 106626.

[11] M. Mirz, "A dynamic phasor real-time simulation based digital twin for power systems; 1. Auflage," *Ph.D. dissertation, RWTH Aachen Univ.*, Aachen, Germany, 2020.

[12] J. Dinkelbach, G. Nakti, M. Mirz, and A. Monti, "Simulation of low inertia power systems based on shifted frequency analysis," *Energies*, vol. 14, no. 7, p. 1860, Mar. 2021.

[13] A. Nazari, Y. Xue, J. K. Motwani, I. Cvetkovic, D. Dong, and D. Boroyevich, "Dynamic phasor modeling of multi-converter systems," in *Proc. IEEE Energy Convers. Congr. Expo. (ECCE)*, Oct. 2021, pp. 2716–2721.

[14] W. Si, C. Liu, S. Liu, H. Li, C. Zhang, and J. Fang, "Dynamic phasor modeling of single-phase grid-forming converters," 2024, *arXiv:2404.11304*.

[15] F. Hossain and N. R. Chaudhuri, "A dynamic phasor framework for analysis of grid-forming converter connected to series-compensated line," in *Proc. IEEE Power Energy Soc. Gen. Meeting (PESGM)*, Jul. 2025, pp. 1–5.

[16] M. Mirz, J. Dinkelbach, and A. Monti, "DPsim—Advancements in power electronics modelling using shifted frequency analysis and in real-time simulation capability by parallelization," *Energies*, vol. 13, no. 15, p. 3879, Jul. 2020.

[17] S. Peiris, S. Filizadeh, and D. Muthumuni, "Modular dynamic phasor modeling and simulation of renewable integrated power systems," *Energies*, vol. 17, no. 11, p. 2480, May 2024.

[18] R. G. Azevedo, S. Gomes, and T. J. M. A. Parreiras, "Dynamic phasor model of HVDC links for linear analysis of dynamic performance," *Int. J. Electr. Power Energy Syst.*, vol. 160, Sep. 2024, Art. no. 110101.

[19] S. Alsarayreh, R. Dimitrovski, and A. Lekić, "DQsym: A MATLAB/simulink library for dynamic phasor simulation of AC/DC power systems," *SoftwareX*, vol. 34, Jun. 2026, Art. no. 102719. [Online]. Available: https://www.sciencedirect.com/science/article/pii/S2352711026002116

[20] X. Mao, H. Luo, W. Zhong, L. Wu, and Z. Yuan, "Modeling and application of DQ-sequence dynamic phasors under unbalanced AC conditions," *Int. J. Electr. Power Energy Syst.*, vol. 166, May 2025, Art. no. 110524. [Online]. Available: https://linkinghub.elsevier.com/retrieve/pii/S0142061525000754